Numerical simulations of concrete specimens with the gradient-enhanced Eikonal non-local damage model

Breno Ribeiro Nogueira [1,2] , Giuseppe Rastiello [3], Cédric Giry [1], Fabrice Gatuingt [1], Carlo Callari [2]

[1] Université Paris-Saclay, CentraleSupelec, ENS Paris-Saclay, CNRS, LMPS - Laboratoire de Mécanique Paris-Saclay

[2] Università degli Studi del Molise, DiBT

[3] Université Paris-Saclay, CEA, Service d'etudes mécaniques et thérmiques

Corresponding author: Breno Ribeiro Nogueira (e-mail: breno.ribeiro_nogueira@ens-paris-saclay.fr)

ABSTRACT Accurately predicting the response of structures subjected to complex loadings is a challenging task in civil engineering. In particular, studying cracking nucleation and propagation is essential to assess structural performances. Quasi-brittle materials, such as concrete, are generally modeled using strain-softening constitutive models. According to Continuum Damage Mechanics, material degradation is represented at a macroscopic level by a scalar or tensorial damage variable. However, the strong localization of the mechanical fields leads to mesh-dependent finite element numerical simulations. To recover the objectivity of the results, damage models need to be regularized. Numerous techniques have been proposed (e.g., non-local models, phase-field formulations, micromorphic medium, etc.), acting as localization limiters. This work concentrates on one class of regularization methods: the so-called non-local damage models of gradient type. This paper applies the eikonal gradient-enhanced model to the simulation of experimental tests in a few concrete specimens. Results are provided in terms of the structural response and of the damage maps.

Keywords Damage, non-local, quasi-brittle, gradient-enhanced, eikonal formulation

I. INTRODUCTION

In a finite element context, regularization methods should be applied if one seeks to model the behavior of quasi-brittle materials (e.g., concrete). Several localization limiters exist in the literature (e.g., Pijaudier-Cabot & Bažant (1987), Peerlings et al. (1996), Bourdin et al. (2000), Nedjar (1995), Moës et al. (2011), Moës & Chevaugeon (2021)) sharing the introduction in the formulation of an internal length scale. The classic integral non-local approach (Pijaudier-Cabot & Bažant 1987) can regularize the response by averaging a local field in a zone defined by an internal (or characteristic) length. An equivalent (and more computationally efficient) approach is to compute the non-local field driving damage evolution by solving an additional Helmholtz-type differential equation (Peerlings et al. 1996). In both cases, mesh objectivity is restored in terms of structural response. Still, some drawbacks (e.g., damage diffusion across highly damaged regions and boundary effects) make it challenging to predict realistic crack paths.

The nonphysical damage bands initiation and evolution for these models in some specific situations has already been studied in several works (Simone et al. 2004, Krayani et al. 2009, Geers et al. 1998). Such an issue is related to the primary assumption of considering constant and isotropic non-local interactions throughout the damage process. Non-local models considering evolving interactions (e.g., (Geers et al. 1998,

Pijaudier-Cabot & Dufour 2010, Giry et al. 2011, Nguyen 2011, Desmorat et al. 2015, Vandoren & Simone 2018)) may be capable of reproducing more realistic results.

This paper focuses on two different gradient-enhanced non-local models: the classic implicit gradient (Peerlings et al. 1996) and the gradient version of the Eikonal approach (Desmorat et al. 2015). Firstly, the boundary value problem for both models is recalled, highlighting their theoretical differences. Then, two numerical examples are used to compare the performances of the approaches in terms of structural response and damage maps.

II. BEHAVIOR

The basic assumption of non-locality is that the principle of local action issued from continuum mechanics is no longer valid. In certain materials, the microstructure strongly influences the macroscopic behavior. Consequently, constitutive relations should consider what happens in the entire body. In Continuum Damage Mechanics (CDM), non-locality can be seen as the macroscopic result of the different interactions between microcracks. For integral type models (Pijaudier-Cabot & Bažant 1987), a common choice is to apply a weighted average to the variable controlling damage evolution (see, e.g., Jirásek (1998)), e.g., an equivalent strain measure. Conversely, in gradient formulation, the non-local field is computed by solving a Helmholtz equation (Peerlings 1999).

In this work, an isotropic damage model with a single scalar damage variable D is considered. The constitutive relation reads:

$$\boldsymbol{\sigma} = (1 - D)\mathbb{E} : \boldsymbol{\varepsilon} \tag{1}$$

where $\boldsymbol{\sigma}$ is the Cauchy's second-order stress tensor, $\mathbb{E}$ is the fourth-order Hooke's tensor and $\boldsymbol{\varepsilon}$ is the small strains second-order tensor.

Damage ranges from the state of undamaged material ($D = 0$) to fully damaged ($D = 1$) according to the following equation:

$$D = 1 - \frac{\kappa_0}{\kappa}\left(1 - \alpha + \alpha e^{-B(\kappa - \kappa_0)}\right) \tag{2}$$

where:

$$\kappa = \max_t(\kappa_0, \bar{e}) \tag{3}$$

is a damage-driving history variable, $\bar{e}$ is the non-local equivalent strain, κ_0 is the damage threshold and B the damage brittleness. The parameter α is used to account for residual stresses in the behavior law.

In this work, the local equivalent strain is defined by the modified Von Mises model (de Vree et al. 1995) and reads:

$$e = \frac{k-1}{2k(1-2\nu)} I_1 + \frac{1}{2k}\sqrt{\frac{(k-1)^2}{(1-2\nu)^2} I_1^2 + \frac{12k}{(1+\nu)^2} J_2'} \tag{4}$$

where ν is the Poisson's ratio, and k is a parameter corresponding to the ratio of the material strength in compression and in tension. The invariants of the strain tensor are defined as:

$$I_1 = \mathrm{Tr}(\boldsymbol{\varepsilon}) \tag{5}$$

$$J_2' = \frac{1}{6}\left(3\mathrm{Tr}(\boldsymbol{\varepsilon} \cdot \boldsymbol{\varepsilon}) - \mathrm{Tr}^2(\boldsymbol{\varepsilon})\right) \tag{6}$$

III. GRADIENT-ENHANCED NON-LOCAL DAMAGE MODELS

In the case of the classic non-local integral model, a convolution product between the local equivalent strain field and a weighting function is used to compute the non-local equivalent strain. An equivalent gradient

non-local approach can be obtained from the classic integral one (Peerlings et al. 1996). The main difference is that the equilibrium differential equation is coupled with a diffusion one, controlling the non-local equivalent strain field. Other models exist where the damage variable is considered to respect a diffusion equation (see, e.g., (Nedjar 1995, Bourdin et al. 2000, Miehe et al. 2010)).

A. GNL damage model

For the classic implicit gradient model, the Helmholtz differential equation to be solved to compute $\bar{e}$ and its boundary condition read:

$$\bar{e} - c\nabla^2\bar{e} = e \qquad \text{on } \Omega \tag{7}$$

$$\nabla\bar{e}\cdot\boldsymbol{n} = 0 \qquad \text{on } \partial\Omega \tag{8}$$

where Ω is the considered body, $\partial\Omega$ denotes its boundary, $\boldsymbol{n}$ is the outward normal vector to $\partial\Omega$, and c is the gradient parameter homogeneous to the square of a length.

B. ENLG damage model

Similarly, the gradient version of the ENL model can be obtained from its integral counterpart in the space curved by damage (Desmorat et al. 2015). In a general anisotropic CDM context, evolving non-local interactions are considered by introducing a Riemannian metric $\mathbf{g} = (\mathbf{I} - \mathbf{D})^{-1}$, with $\mathbf{I}$ denoting the second-order identity tensor and $\mathbf{D}$ the second-order anisotropic damage tensor. The modified Helmholtz problem to be solved then reads:

$$\bar{e} - c\frac{1}{\sqrt{\det\mathbf{g}}}\nabla\cdot\left(\sqrt{\det\mathbf{g}}\,\mathbf{g}^{-1}\cdot\nabla\bar{e}\right) = e \qquad \text{on } \Omega \tag{9}$$

$$\mathbf{g}^{-1}\cdot\nabla\bar{e}\cdot\boldsymbol{n} = 0 \qquad \text{on } \partial\Omega \tag{10}$$

A full two-dimensional (2D) isotropic simplification of this model can be obtained by considering the metric $\mathbf{g} = \mathbf{I}'/(1-D)$, with $\mathbf{I}'$ denoting the 2D identity tensor. Thus, one has $\det\mathbf{g} = 1/(1-D)^2$ and $\mathbf{g}^{-1} = (1-D)\mathbf{I}'$, and the previous differential problem becomes:

$$\bar{e} - c(1-D)\nabla^2\bar{e} = e \qquad \text{on } \Omega \tag{11}$$

$$(1-D)\nabla\bar{e}\cdot\boldsymbol{n} = 0 \qquad \text{on } \partial\Omega \tag{12}$$

One should notice that when $D \to 1$, the non-local equivalent strain equals its local counterpart, which is the desired behavior of vanishing non-local interactions upon localization. The first numerical implementations of the integral and gradient versions of this model can be found in (Rastiello et al. 2018, Thierry et al. 2020, Thierry 2021, Marconi 2022, Ribeiro Nogueira et al. 2022).

IV. NUMERICAL FORMULATION

A. Boundary value problem (variational form)

Let us introduce the following functional spaces:

$$\mathcal{U}(\boldsymbol{u}^d) = \{\boldsymbol{w} \mid \boldsymbol{w} \in H^1(\Omega)\ ,\ \boldsymbol{w} = \boldsymbol{u}^d \text{ on } \partial\Omega_u\} \tag{13}$$

$$\mathcal{U}(\mathbf{0}) = \{\boldsymbol{w} \mid \boldsymbol{w} \in H^1(\Omega)\ ,\ \boldsymbol{w} = \mathbf{0} \text{ on } \partial\Omega_u\} \tag{14}$$

$$\mathcal{V} = \{w \mid w \in H^1(\Omega)\} \tag{15}$$

where $\boldsymbol{u}^d$ is the imposed displacement on $\partial\Omega_u$.

Neglecting body forces, and under quasi-static conditions, the fully 2D variational damage mechanics problem to be solved consists in finding at each time t, the admissible displacement field $\boldsymbol{u} \in \mathcal{U}(\boldsymbol{u}^d)$ and the admissible non-local equivalent strain field $\bar{e} \in \mathcal{V}$ satisfying:

$$\int_\Omega (1-D)\boldsymbol{\varepsilon}(\boldsymbol{u}) : \mathbb{E} : \boldsymbol{\varepsilon}(\boldsymbol{v})\, dV = \int_{\partial\Omega_t} \boldsymbol{t}^d \cdot \boldsymbol{v}\, dS \qquad \forall\, \boldsymbol{v} \in \mathcal{U}(\boldsymbol{0}) \tag{16}$$

$$\int_\Omega \frac{1}{1-D}\, \bar{e}\, \eta dV + \int_\Omega c\nabla\bar{e} \cdot \nabla\eta dV = \int_\Omega \frac{1}{1-D}\, e\, \eta dV \qquad \forall \eta \in \mathcal{V} \tag{17}$$

where $\boldsymbol{\varepsilon}(\boldsymbol{u})$ (respectively, $\boldsymbol{\varepsilon}(\boldsymbol{v})$) is the small strain tensor applied to $\boldsymbol{u}$ (respectively, $\boldsymbol{v}$), $\boldsymbol{v}$ is a virtual displacement field, η is a virtual equivalent strain field, and $\boldsymbol{t}^d$ is the imposed traction vector on $\partial\Omega_t$.

B. Finite element formulation

The computational domain Ω is discretized through a finite element mesh Ω^h containing triangular elements. The unknown displacement and non-local equivalent strain fields on each finite element are approximated by linear interpolation of their nodal values (denoted by the piecewise polynomials $\mathbb{P}_1$). Drawing from (Badri et al. 2021, Badri & Rastiello 2023), a staggered Picard iteration algorithm is employed to handle non-linearity and the displacement control is used. At iteration $k+1$, one first computes the $[\mathbb{P}_1, \mathbb{P}_1]$ discretized vector-valued displacement field $\boldsymbol{u}^{h,k+1} \in \mathcal{U}^h(\boldsymbol{u}^d)$ such that:

$$\int_{\Omega^h} (1-D^{h,k})\boldsymbol{\varepsilon}(\boldsymbol{u}^{h,k+1}) : \mathbb{E} : \boldsymbol{\varepsilon}(\boldsymbol{v}^h)\, dV = \int_{\partial\Omega_t^h} \boldsymbol{t}^d \cdot \boldsymbol{v}^h\, dS \;\; \forall\, \boldsymbol{v}^h \in \mathcal{U}^h(\boldsymbol{0}) \tag{18}$$

and then computes the $\mathbb{P}_1$ discretized nonlocal equivalent strain field $\bar{e}^{h,k+1}$ solving:

$$\int_{\Omega^h} \frac{1}{1-D^{h,k}}\, \bar{e}^{h,k+1}\, \eta^h dV + \int_{\Omega^h} c\nabla\bar{e}^{h,k+1} \cdot \nabla\eta^h dV = \int_{\Omega^h} \frac{1}{1-D^{h,k}}\, e(\boldsymbol{\epsilon}(\boldsymbol{u}^{h,k+1}))\, \eta^h dV \;\; \forall \eta \in \mathcal{V}^h \tag{19}$$

Here, ($\mathcal{U}^h(\boldsymbol{u}^d)$, $\mathcal{U}^h(\boldsymbol{0})$, $\mathcal{V}^h$) are the discretized counterparts of ($\mathcal{U}(\boldsymbol{u}^d)$, $\mathcal{U}(\boldsymbol{0})$, $\mathcal{V}$), $D^{h,k}$ is the $\mathbb{P}_0$ (constant inside an element) discretized damage field at iteration k, and $e(\boldsymbol{\epsilon}(\boldsymbol{u}^{h,k+1}))$ is the $\mathbb{P}_0$ local strain field computed from the symetrized gradient of $\boldsymbol{u}^{h,k+1}$. At each iteration, the field $\bar{e}^{h,k+1}$ is used to update the $\mathbb{P}_0$ history variable field κ^h and compute damage. The solution is repeated till convergence at each pseudo-time step.

V. NUMERICAL RESULTS

Two simple test cases are illustrated in the following to show the main differences between the GNL and ENLG damage formulations regarding damage evolution and mesh sensitivity of the overall structural response. In particular, attention is focused on damage propagation on a L-shape panel (Winkler et al. 2001, 2004) and a double notched specimen under tension (Shi et al. 2000).

Almost the same model parameters (i.e., B, c, α, etc.) are used for both simulations so that one can compare the models under the same conditions. The structural response and the cracking behavior are influenced by this choice. For instance, increasing B leads to more brittle responses, and decreasing c can affect how fast the crack propagates. The recalibration of these parameters is essential when one seeks to represent entirely consistent experimental results, considering the real boundary conditions applied. This is beyond the scope of this work and is left for future work.

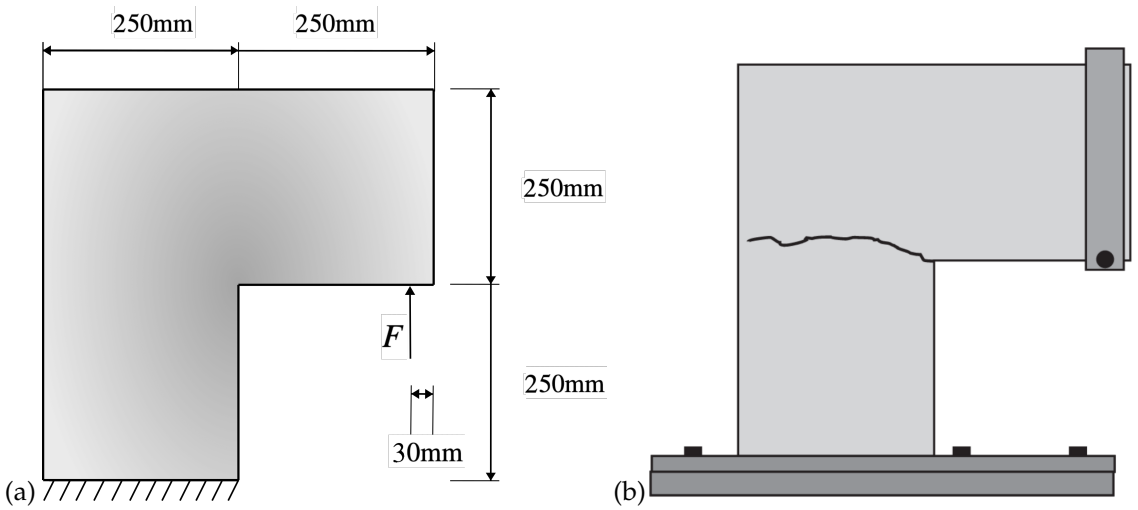

FIGURE 1. L-shape test: (a) Geometry (thickness = 100mm), boundary and loading conditions; (b) Experimental crack-path.

A. L-shape test

The first example considered is the L-shape concrete panel test presented in (Winkler et al. 2001, 2004). Geometry and boundary conditions are depicted in figure 1a. The material parameters used for the simulation are the following: Young's modulus $E = 25.85$ GPa, Poisson's ratio $\nu = 0.18$, damage threshold $\kappa_0 = 1.2\text{x}10^{-4}$, strength ratio $k = 10$, damage evolution parameter $B = 300$, gradient parameter $c = 4$ mm^2 and parameter $\alpha = 0.99$. Two different finite element meshes with 14992 and 23301 Constant Strain Triangle (CST) elements were used for this problem.

The structural response (force vs. displacement curve) is given in figure 2. It is shown that the ENLG model provides a more brittle response when compared to the GNL one. This is, in fact, expected for such models considering evolving non-local interactions. Mesh convergence is obtained, but due to minor oscillations in the non-local equivalent strain field (and consequently in damage), the ENLG response may show slightly different curves upon mesh refinement. This behavior is typical of gradient damage models with evolving non-local interactions (Vandoren & Simone 2018) and should be further studied.

Figure 3 shows the damage profile obtained for the GNL and ENLG models. An excellent agreement between the "pseudo-crack" path described by the ENLG model and the experimental one (see 1b) is obtained. One can see that the GNL model gives a larger damage band when compared to ENLG. Furthermore, the damage is not concentrated in a line (representative of the expected damage-to-fracture transition) due to the damage spreading. The ENLG model gives, in this case, a more realistic damaging behavior.

B. Shi-test

The second example studied is the concrete notched specimen described in (Shi et al. 2000), the so-called Shi-test. Material parameters are exactly the same as before, except for Young's modulus and Poisson's ratio, which are here: $E = 24$ GPa and $\nu = 0.2$. Geometry and boundary conditions are depicted in figure 4. Two meshes containing 7006 and 19384 CST elements were used for the simulations.

Figure 5 shows the structural response obtained for both ENLG and GNL models. Once again, the ENLG provides a more brittle response when compared to the GNL model. This behavior is intrinsically

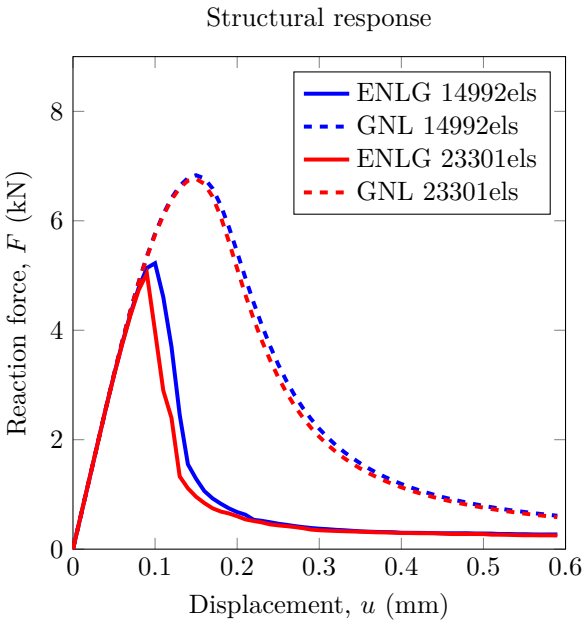

FIGURE 2. L-shape test: mesh convergence and comparison among ENLG (solid lines) and GNL (dashed lines) models.

related to the damage profiles obtained for both models (figure 6b). An "pseudo-crack" (highly damaged zone) appears earlier for the ENLG model and propagates faster than the GNL model. Thus, the structural post-pic behavior rapidly reaches low values for the ENLG model.

Moreover, the ENLG model gives a damage profile that resembles two different "pseudo-crack" propagating from the notches, whereas it remains challenging to identify a "pseudo-crack" path for the GNL model. The same result considering element deletion post-processing is given in figure 6. While the two "pseudo-crack" can be clearly identified for the ENLG model, the GNL one shows two larger zones which cannot be really related to a cracking behavior (figure 6b). A similar result can be obtained when the applied displacement is around 0.02 mm (figure 6a). At this stage of the simulation, the ENLG is almost at the end of its quasi-brittle post-pic behavior, so damage is localized and the two different "pseudo-crack" can be already observed. At the same time, the GNL model has just started its post-pic phase, so no effective damage is localized and the cracking zone cannot be identified. Furthermore, damage is mostly localized in one line of elements for the ENLG model. This cracking zone becomes slightly bigger throughout the rest of the analysis.

VI. CONCLUSION

A brief overview of the GNL and ENLG damage models has been presented. Numerical examples of well-known concrete benchmarks were used to highlight the performances of both approaches in modeling damaging in concrete specimens. It is shown, as expected, that the classic implicit gradient approach can regularize the response but leads to unrealistic "pseudo-crack" paths due to damage spreading, for instance. Conversely, the ENLG model provided more physical results in terms of damaging behavior and localizes damage in narrow zones. Despite the small oscillations observed in the structural response, convergence was clearly obtained for the problems studied. However, if one aims to represent better the experimental

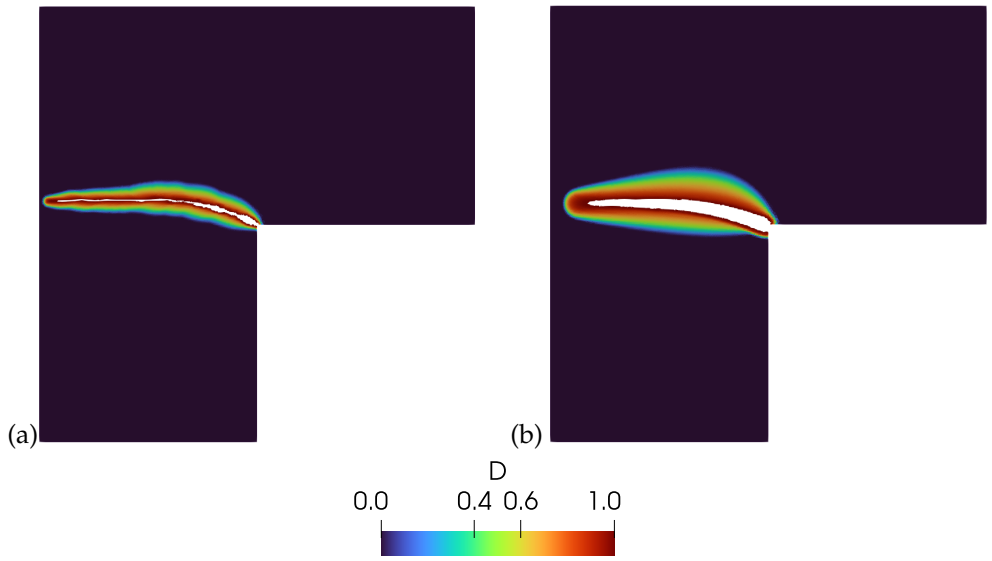

FIGURE 3. L-shape test: comparison of damage profiles for ENLG (a) and GNL (b) considering element deletion when $D > 0.995$ for the sake of post-processing.

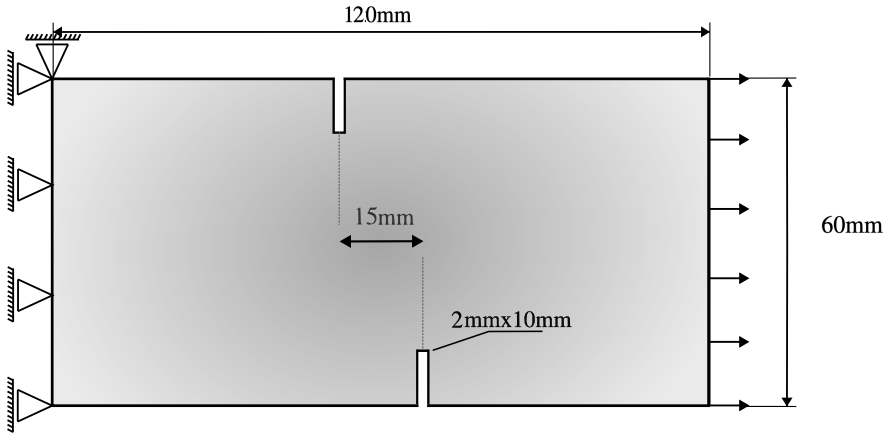

FIGURE 4. Shi-test: Geometry (thickness = 10mm), boundary and loading conditions.

findings, a proper calibration of the model parameters is necessary.

Extension to anisotropic damage is straightforward by using the damage-dependent Riemaniann metric coupled with a convenient behavior law. It should be noticed, however, that close to failure, a transition to an explicit description of the fracture is required. The CDM framework cannot reproduce the real jump in the displacement field nor give more information about crack opening, for instance. In this situation, the ENLG model may provide essential information about localization, such as the zones (and directions) where a discontinuity should be introduced (see for instance Simone et al. (2003)). This could allow using some explicit approaches (e.g., in the Embedded Finite Element Method, E-FEM) without additional tracking algorithms.

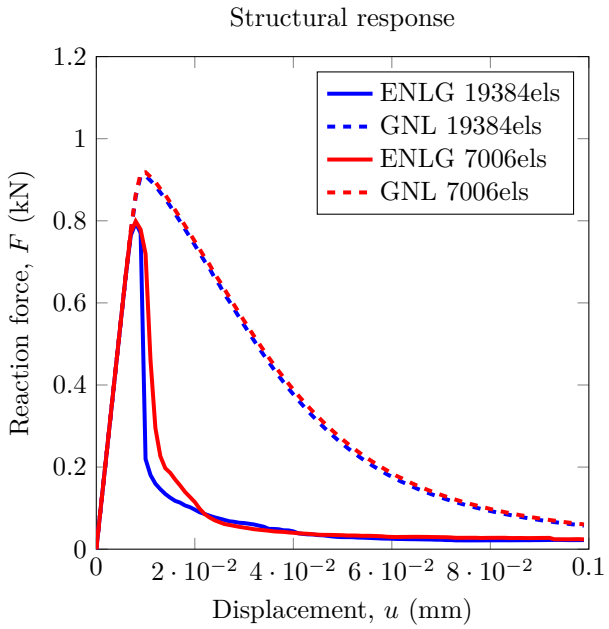

FIGURE 5. Shi-test: mesh convergence and comparison among ENLG (solid lines) and GNL (dashed lines) models.

References

Badri, M. A. & Rastiello, G. (2023), Hpc finite element solvers for phase-field models for fracture in solids, *in* P. Rossi & J.-L. Tailhan, eds, 'Numerical Modeling Strategies for Sustainable Concrete Structures', Springer International Publishing, Cham, pp. 22–32.

Badri, M. A., Rastiello, G. & Foerster, E. (2021), 'Preconditioning strategies for vectorial finite element linear systems arising from phase-field models for fracture mechanics', *Computer Methods in Applied Mechanics and Engineering* **373**, 113472.

Bourdin, B., Francfort, G. & Marigo, J.-J. (2000), 'Numerical experiments in revisited brittle fracture', *Journal of the Mechanics and Physics of Solids* **48**(4), 797–826.

de Vree, J. H. P., Brekelmans, W. A. M. & van Gils, M. A. J. (1995), 'Comparison of nonlocal approaches in continuum damage mechanics', *Computers & Structures* **55**(4), 581–588.

Desmorat, R., Gatuingt, F. & Jirásek, M. (2015), 'Nonlocal models with damage-dependent interactions motivated by internal time', *Engineering Fracture Mechanics* **142**, 255–275.

Geers, M., de Borst, R., Brekelmans, W. & Peerlings, R. (1998), 'Strain-based transient-gradient damage model for failure analyses', *Computer Methods in Applied Mechanics and Engineering* **160**(1-2), 133–153.

Giry, C., Dufour, F. & Mazars, J. (2011), 'Stress-based nonlocal damage model', *International Journal of Solids and Structures* **48**(25-26), 3431–3443.

Jirásek, M. (1998), 'Nonlocal models for damage and fracture: Comparison of approaches', *International Journal of Solids and Structures* **35**(31-32), 4133–4145.

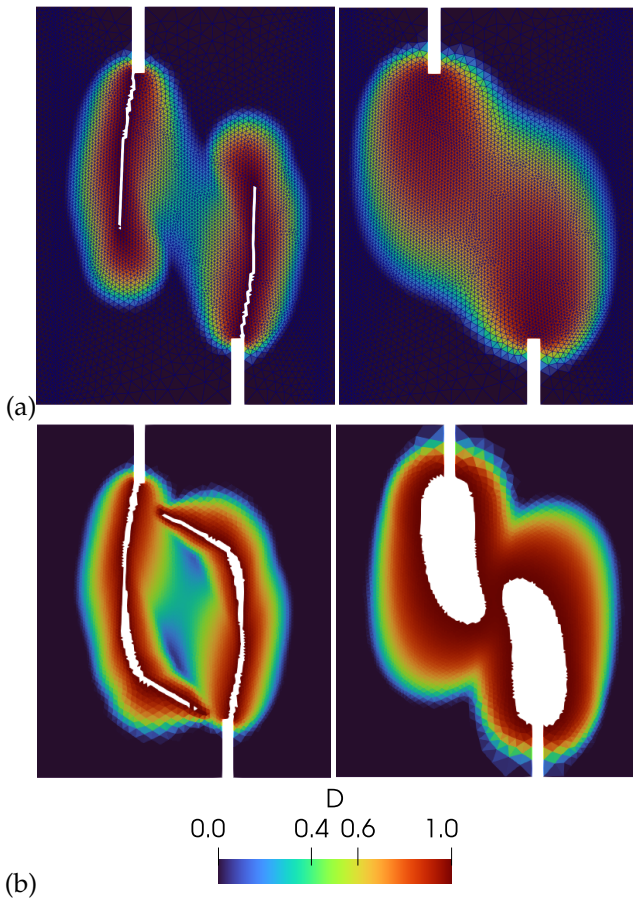

FIGURE 6. Shi-test: comparison of damage profiles for ENLG (left) and GNL (right) considering element deletion when $D > 0.992$ for the sake of post-processing. (a) Displacement of around 0.2 mm; (b) end of the simulation.

Krayani, A., Pijaudier-Cabot, G. & Dufour, F. (2009), 'Boundary effect on weight function in nonlocal damage model', *Engineering Fracture Mechanics* **76**(14), 2217–2231.

Marconi, F. (2022), Damage-fracture transition by an Eikonal-based gradient-type formulation for damage (-plastic) model, PhD thesis, Université Paris-Saclay, ENS Paris-Saclay.

Miehe, C., Welschinger, F. & Hofacker, M. (2010), 'Thermodynamically consistent phase-field models of fracture: Variational principles and multi-field FE implementations', *International Journal for Numerical Methods in Engineering* **83**(10), 1273–1311.

Moës, N. & Chevaugeon, N. (2021), 'Lipschitz regularization for softening material models: the Lip-field approach', *Comptes Rendus. Mécanique* **349**(2), 415–434.

Moës, N., Stolz, C., Bernard, P.-E. & Chevaugeon, N. (2011), 'A level set based model for damage growth: The thick level set approach', *International Journal for Numerical Methods in Engineering* **86**(3), 358–380.

Nedjar, B. (1995), Mécanique de l'endommagement. Théorie du premier gradient et application au béton, PhD thesis, Ecole Nationale des Ponts et Chaussées.

Nguyen, G. D. (2011), 'A damage model with evolving nonlocal interactions', *International Journal of Solids and Structures* **48**(10), 1544–1559.

Peerlings, R., de Borst, R., Brekelmans, W. & de Vree, J. (1996), 'Gradient-enhanced damage model for quasi-brittle materials.', *International Journal for Numerical Methods in Engineering* **39**, 391–403.

Peerlings, R. H. J. (1999), Enhanced damage modelling for fracture and fatigue, PhD thesis, Technische Universiteit Eindhoven.

Pijaudier-Cabot, G. & Dufour, F. (2010), 'Non local damage model: Boundary and evolving boundary effects', *European Journal of Environmental and Civil Engineering* **14**(6-7), 729–749.

Pijaudier-Cabot, G. & Bažant, Z. P. (1987), 'Nonlocal damage theory', *Journal of Engineering Mechanics* **113**(10), 1512–1533.

Rastiello, G., Giry, C., Gatuingt, F. & Desmorat, R. (2018), 'From diffuse damage to strain localization from an Eikonal Non-Local (ENL) Continuum Damage model with evolving internal length', *Computer Methods in Applied Mechanics and Engineering* **331**, 650–674.

Ribeiro Nogueira, B., Giry, C., Rastiello, G. & Gatuingt, F. (2022), 'One-dimensional study of boundary effects and damage diffusion for regularized damage models', *Comptes Rendus. Mécanique* **350**(G3), 507–546.

Shi, C., van Dam, A. G., van Mier, J. G. & Sluys, B. (2000), Crack Interaction in Concrete, *in* F. H. Wittmann, ed., 'Materials for Buildings and Structures', Wiley-VCH Verlag GmbH & Co. KGaA, Weinheim, FRG, pp. 125–131.

Simone, A., Askes, H. & Sluys, L. J. (2004), 'Incorrect initiation and propagation of failure in non-local and gradient-enhanced media', *International Journal of Solids and Structures* **41**(2), 351–363.

Simone, A., Wells, G. N. & Sluys, L. J. (2003), 'From continuous to discontinuous failure in a gradient-enhanced continuum damage model', *Computer Methods in Applied Mechanics and Engineering* **192**(41-42), 4581–4607.

Thierry, F. (2021), Modélisation de la localisation des déformations dans les milieux adoucissants par une approche eikonale, PhD thesis, Université Paris-Saclay, ENS Paris-Saclay.

Thierry, F., Rastiello, G., Giry, C. & Gatuingt, F. (2020), 'One-dimensional Eikonal Non-Local (ENL) damage models: Influence of the integration rule for computing interaction distances and indirect loading control on damage localization', *Mechanics Research Communications* **110**.

Vandoren, B. & Simone, A. (2018), 'Modeling and simulation of quasi-brittle failure with continuous anisotropic stress-based gradient-enhanced damage models', *Computer Methods in Applied Mechanics and Engineering* **332**, 644–685.

Winkler, B., Hofstetter, G. & Lehar, H. (2004), 'Application of a constitutive model for concrete to the analysis of a precast segmental tunnel lining', *International Journal for Numerical and Analytical Methods in Geomechanics* **28**(7-8), 797–819.

Winkler, B., Hofstetter, G. & Niederwanger, G. (2001), 'Experimental verification of a constitutive model for concrete cracking', **215**, 12.